Genetically-engineered anti-PSMA exosome mimetics targeting advanced prostate cancer in vitro and in vivo

Queen's University Belfast - Research Portal:
Link to publication record in Queen's University Belfast Research Portal

Genetically-Engineered Anti-PSMA Exosome Mimetics Targeting Advanced Prostate Cancer *In Vitro* and *In Vivo*

Maja Severic†[1], Guanglong Ma†[1], Sara Pereira[1], Amalia Ruiz[1], Calvin C.L. Cheung[1], and Wafa T. Al-Jamal[1]

† Both authors equally contributed to this manuscript

[1]School of Pharmacy, Queen's University Belfast, United Kingdom

*Corresponding author:

Dr Wafa' T. Al-Jamal

School of Pharmacy

Queen's University Belfast

Belfast, BT9 7BL

United Kingdom

E-mail: w.al-jamal@qub.ac.uk

Abstract

The present work describes the engineering of anti-PSMA peptide-decorated exosome mimetics (EMs) targeting advanced prostate cancer (PC). The targeted EMs were produced from anti-PSMA peptide, WQPDTAHHWATL, expressing U937 monoblastic cells, followed by successive extrusion cycles. The engineered EMs were nanosized, produced at a high yield, and displayed the anti-PSMA peptide, exosomal markers and monocytes proteins on their surface. As anticipated, PSMA-EMs showed increased cellular internalization in PSMA positive PC cell lines (LNCaP and C4-2B), compared to unmodified EMs. Most importantly, higher tumour targeting was observed in solid C4-2B tumours, following intravenous administration, confirming their targeting ability *in vivo*. Overall, our study indicates that the engineered anti-PSMA peptide-targeted EMs can be a promising drug delivery system for advanced PC.

1. Introduction

Treatment options for prostate cancer (PC) vary based on the stage and type of cancer. Chemotherapy is most widely used to treat the metastatic castration-resistant prostate cancer (mCRPC); however, its efficacy has been limited due to its lack of selectivity and systemic toxicity [1]. Therefore, targeted drug delivery systems could be promising tools to reduce side effects of chemotherapeutics. Prostate-specific membrane antigen (PSMA) is a 100 kDa type II transmembrane glycosylated protein expressed on the prostate epithelial cell membrane, which is overexpressed on PC cells as the disease progresses [2]. Furthermore, PSMA has been found in the tumour neovasculature of various types of solid tumours [3, 4]. PSMA has been extensively used as a targeted antigen in drug delivery systems, where the binding of the PSMA ligand to its receptor on the PC cells triggers receptor-mediated endocytosis, followed by intracellular drug release [5, 6]. Various peptides, aptamers, small-molecules and antibodies have been developed, and conjugated to drugs or nanocarriers to improve their targeting efficiency to PC [7-12]. Furthermore, several PSMA-based diagnostic and therapeutic agents are in clinical trials, implicating that this approach has a great potential in future PC targeted therapies [13-16].

Naturally secreted extracellular vesicles, exosomes, have been widely described as drug delivery systems. Due to their small size (50-100 nm), biocompatibility, natural ability of cellular communication and macromolecules delivery, they have been used in various studies [17]. Exosomes also play a role in tumour growth and metastasis, making them good therapeutic targets and diagnostic/prognostic biomarkers [18]. Exosomes have intrinsic homing abilities, which means that they can target and accumulate in the specific tissues from which they originate [19-21]. However, the main limitations of exosomes as delivery systems are their time-consuming purification and low yield [22]. Recently, new approaches describing bioinspired nanovesicles, such as exosome mimetics [23-25], biomimetics [26] or cell-derived nanovesicles [27-30] have been reported to improve the exosomes yield while retaining their major characteristics. Exosome mimetics (EMs) have been produced by extruding cells through membrane filters, inducing lipid bilayer fragmentation and self-assembly into nanovesicles [29]. Interestingly, the original protein content from the initial cells was preserved on the EMs surface, without affecting their intrinsic targeting capabilities [24, 26]. EMs have been generated from a wide range of cells, including monocytes, mesenchymal stem cells, human embryonic kidney cells and immature dendritic cells, and were utilised in tumour targeting, immunotherapy, siRNA delivery and regenerative medicine [25, 27, 30, 31]. As drug nanocarriers, different chemotherapeutics have been successfully loaded into EMs with superior anti-tumour efficacy *in vitro* and *in vivo* [24, 26, 28, 32, 33]. Exosomes surface functionalisation methods have been widely described in the literature, such as genetic or metabolic engineering, covalent surface chemistry and hydrophobic insertion to

enhance exosomes targeting [34]. In the present work we describe, for the first time, the genetic engineering of anti-PSMA EMs to target advanced PC. To obtain PSMA-targeted EMs, U937 monoblastic cells were transfected by nucleofection or transduced using lentivirus to express anti-PSMA peptide (WQPDTAHHWATL) on their cell membrane, followed by successive extrusion cycles. The peptide expression on cells membrane was confirmed. Furthermore, successful engineering of nanosized, anti-PSMA expressing EMs was achieved, and efficient PSMA-targeting was confirmed *in vitro* and *in vivo* PC models.

2. Materials and methods

Cell culture

Monoblastic cell line U937 (CRL-1593.2™ ATCC®) and prostate cancer C4-2B (MD Anderson Cancer Centre, Texas, USA), LNCaP (CRL-1740™ ATCC®) and PC3 (CRL-1435™ ATCC®) cells were grown in advanced RPMI 1640 medium supplemented with 10% foetal bovine serum (FBS), 1% penicillin-streptomycin and 2mM L-glutamine. All cells were cultured in T-75 tissue culture flasks (Thermo Fisher Scientific, UK) at 37 °C incubator with a humidified atmosphere of 5% CO_2. U937 cells were passaged twice a week using fresh media to maintain cell concentration at 5 x 10^5 cells/mL. C4-2B, LNCaP and PC3 cells were passaged using 0.05% Trypsin-EDTA when reaching 80% confluence to maintain exponential growth.

U937 nucleofection

U937 cells were resuspended at 1 x 10^6 cells/100 µL of Nucleofector™ SF solution (Lonza Group, Switzerland). 2 µg of pDisplay pDNA with cloned WQPDTAHHWATL [12] sequence (**Figure S1.A**) was mixed with the cells and SF buffer in a electroporation cuvette, and pulsed with optimised program for U937 cell line (FS-100). Cuvette was removed from Nucleofector™ 4D device and incubated for 10 min at room temperature. 400 µL of pre-warmed RPMI 1640 complete media was added to the cuvette and incubated at 37 °C for 5 min. After incubation cells were transferred to 24-well plate and incubated in complete media for 48 h at 37 °C, then analysed for transfection efficiency.

Lentivirus packaging and U937 lentiviral transduction

Viral targeting vector was purchased from VectorBuilder™ with cloned PSMA-peptide (WQPDTAHHWATL) display sequence (**Figure S2.A**). Lentiviral particles were produced by co-transfecting HEK 293T cell line with VSV-G (Promega, USA) envelope vector, DVPR (Promega, USA) packaging vector (a kind gift from Dr Niamh Buckley) and 3rd generation transfer vector containing the eGFP-PSMA-peptide sequence. Briefly, 3 x 10^6 HEK 293T cells were seeded overnight in a 10 cm petri dish. The following day, transfection for the lentivirus packaging was performed using Lipofectamine® 2000 (DNA µg: lipofectamine µL – 1:3). Lipofectamine® 2000 (27 µL) was mixed with

500 µL Opti-MEM® media (Gibco) and incubated for 5 min at room temperature. Plasmids were mixed with another 500 µL of Opti-MEM®: VSVG (1.5 µg), DVPR (4.5 µg) and transfer vector (3 µg). Lipofectamine® 2000 was added dropwise to the plasmid mixture and incubated for 20 min at room temperature. Lipofectamine/pDNA complexes were added to the HEK 293T cells and incubated overnight in antibiotic-free media at 37 °C/5% CO_2. At 48 and 72 h post transfection, the cell supernatant was collected and filtered through 0.45 µm PES filter (Millipore™) and used immediately for lentiviral transduction of U937 cells. 2 mL of viral media was added to 1 x 10^6 U937 cells and cultured overnight at 37 °C/5% CO_2. Next day, cells were washed twice in DPBS and grown in complete media supplemented with 2 µg/mL of the selection antibiotic, puromycin. Mixed populations of eGFP positive and negative U937 cells transduced by lentivirus were sorted using FACS BD Aria III™ cell sorter (Becton Dickinson). Prior to sorting, cells were resuspended at a concentration of 10^7 cells/mL in complete media and filtered through 30 µm cell strainer to break any aggregates. Approximately 10^5 eGFP positive cells were separated from the mixed population and cultured in complete media with 2 µg/mL of puromycin.

RNA isolation and cDNA synthesis

Total RNA was isolated from cells using PureLink™ RNA Mini Kit (Invitrogen) according to manufacturer's instructions. Total RNA was dissolved in 50 µL of DEPC-water (Invitrogen) and the concentration and purity were determined spectrophotometrically using a Nanodrop (Thermo Scientific, UK). Samples' absorbance was measured at 260 nm, and 260/280 nm and 260/230 nm ratios were determined. Total RNA (1 µg) was reverse transcribed using Superscript® IV First-Strand cDNA Synthesis Reaction (Invitrogen), following manufacturer's instructions.

Real-time PCR

Real-time PCR was carried out using Roche LightCycler 480 (Roche Diagnostics). For each 10 µL real-time PCR (RT-qPCR) reaction, 5 µM of forward primer (5' GACAGACACACTCCTGCTATG 3'), 5 µM of reverse primer (5' CCCAGCATAATCTGGAACATCA 3'), 5 µl of SYBR Green I master mix (Roche Diagnostics), 1.5 µl of cDNA and 2.5 µl of RNAse free water was mixed inside the well. The following conditions were used: an initial denaturation step at 95 °C for 5 min, 40 cycles of denaturation at 95 °C for 10 s, annealing/extension at 60 °C for 10 s. Each PCR run included triplicates of each sample and a negative control without a template. Relative values were obtained from the threshold PCR cycle number (CT, cycle threshold). Relative mRNA levels in each sample were obtained through normalisation to its ACTB (used as an internal standard) content and the comparative CT method was used. Results were expressed as a fold-change, which is given by $2^{-\Delta\Delta CT}$, where $\Delta\Delta CT = \Delta CT$ target gene - ΔCT control.

Western blot

For SDS-PAGE, samples were lysed in 2% SDS RIPA buffer and 8 M urea, and diluted in a loading buffer (150 mM Tris-HCl (pH 6.8), 6% SDS, 1.5% 2-mercaptoethanol, 0.3% bromophenol blue, and 30% glycerol) to achieve a final protein amount of 20 µg (as measured by BCA assay, Thermo Scientific). Samples were incubated at 37 °C for 30 min, and 40 µL of sample was loaded into each well. Proteins were separated on 10 and 16% SDS-PAGE gel in Tris-Glycine-SDS running buffer in Mini-PROTEAN Tetra cell system (Bio-Rad) at 100 V for 2 h. Proteins were transferred to 0.2 µm PVDF membrane (VWR) using Mini Trans-Blot cell (Bio-Rad) in a transfer buffer (25 mM Tris, 192 mM glycine, 20% Methanol, 0.1% SDS) for 1 h at 30 V and 4 °C. After the transfer, membranes were washed in TBST (50 mM Tris-Cl, pH 7.5, 150 mM NaCl, 0.1% Tween 20) for 5 min and blocked in 5% non-fat milk/TBST for 1.5 h at room temperature. Membranes were washed again in TBST for 10 min and probed using primary antibodies against LFA-1 (1:1000, ab13219 Abcam), Moesin (1:10000, ab169789 Abcam), Tsg101 (1:1000, ab125011 Abcam), CD63 (1:1000, ab134045 Abcam), HA-Tag (1:1000, 3724S Cell signalling) and beta-actin (1:1000, 4967S Cell Signalling) at 4 °C overnight. Membranes were washed three times using TBST buffer, then incubated with secondary horseradish peroxidase (HRP)-conjugated anti-rabbit IgG (1:1000, 7074 Cell Signalling) or anti-mouse IgG (1:1000, 7076 Cell Signalling) for 1 h at room temperature. The membranes were washed again three times for 5 min using TBST buffer and analysed with Amersham™ ECL™ Start Western Blotting Reagent (GE Healthcare) and ChemiDoc ™ MP (Bio-Rad).

Preparation of exosome mimetics (EMs)
U937 or anti-PSMA transfected U937 cells were washed three times with PBS, centrifuged for 5 min at 1500 rpm (Heraeus Megafuge 8R, Thermo Scientific, UK), and resuspended in PBS at a concentration of 5×10^6 cells/ mL. Cell suspensions were sequentially extruded through 10 µm (10x); 5 µm (10x); 1 µm (10x); 0.4 µm (10x); 0.2 µm (5x) and 0.1 µm (5x) polycarbonate membrane filters (Whatman) using the mini-extruder (Avanti Polar Lipids, AL USA). To purify EMs from soluble proteins, 500 µL of extruded EMs sample was loaded to a qEV column (Izon Science). As the EMs sample entered the column top filter, more PBS was added, and 500 µL fractions were collected. The first six fractions (3 mL) are considered as the void volume and did not contain any EMs. Fractions 7, 8, 9 and 10 which contain pure EMs were collected and concentrated using Amicon Ultra-4 10k MWCO tubes (Sigma Aldrich, UK). PSMA-EMs-N and PSMA-EMs-L refer to EMs prepared from PSMA-peptide expressing U937 cells engineered using nucleofection and lentiviral transduction, respectively.

EMs characterisation
Hydrodynamic diameter and polydispersity index of the EMs, PSMA-EMs-N and PSMA-EMs-L were studied using dynamic light scattering (DLS) and zeta-potential was measured by laser Doppler electrophoresis with a Zetasizer ZS90 (Malvern). The particle size and concentration were determined

using nanoparticle tracking analysis (NTA) NanoSight NS300 (Malvern). Samples for transmission electron microscopy (TEM) were fixed in PHEM (F/G) buffer (2.5% formadehyde and 2.5% glutaraldehyde in PHEM buffer (0.2 M, pH=7.2) for 15 min. 20 µL of each sample was fixed in 180 µL of PHEM (F/G) buffer. 5 µl of the fixed sample was added to 300 mesh copper grid for 10 sec, and dried using filter paper. Next, 50 µL of deionised water was spotted on a piece of parafilm, and the grid was placed on the top of the water surface, then dried using a filter paper. The washing step was repeated twice, and the grid was left to air dry. Then 20 µL of 2% uranyl acetate was spotted on a piece of parafilm, and the grid was placed on the top to stain the grid for 3-4 min, then the grid was dried using a filter paper. At last, the grid was washed, as described above, with 50 µL of methanol/water (50/50, v/v). The grid was then dried using a filter paper and left to dry in air. All grids were imaged at 120 kV with JEOL JEM-1400Plus transmission electron microscope.

Preparation of DiI labelled EMs
U937 cells (wild type and anti-PSMA-expressing) were resuspended in PBS at the concentration of 5×10^6 cells/mL, and incubated with 20 µM DiI at 37 °C and 100 rpm for 30 min. After incubation, the cells were extruded through different pore size membranes, as previously described, and purified form free DiI and proteins using a qEV column (Izon Science). Fractions containing Dil-labelled EMs were collected and concentrated using Amicon Ultra-4 10k centrifugal filter. Fluorescence intensity of the labelled EMs was measured using FLUOstar® Omega plate reader (excitation and emission wavelength of 244 nm and 590 nm). The final concentration of EMs was measured using the NTA. DiI labelling was assessed before every cellular binding and uptake experiment, and all samples had similar fluorescence intensity and particles concentration (Figure S6).

Binding studies of targeted EMs to recombinant human PSMA protein
Purified recombinant human PSMA/FOLH1 protein (R&D Systems) was immobilised in the wells of 96-well high bind ELISA plate (1 µg/mL, 50 µL/well) by adsorption overnight at 4 °C. Next, 200 µL of blocking buffer (1% BSA/PBS) was added to wells to block non-specific protein binding for 2 h at room temperature. DiI labelled EMs, PSMA-EMs-N and PSMA-EMs-L were resuspended in a binding buffer (50 mM Tris, pH 8, 150 mM NaCl, 1 mM $MgCl_2$, 1 mM $CaCl_2$) at a final concentration of $\sim 3.5 \times 10^{10}$ particles/mL, and added to the wells (200 µL/well). After 2 h incubation at room temperature, the unbound EMs were removed by washing the wells two times with 200 µL of binding buffer. Bound EMs were then quantified by determining the fluorescence intensity at an excitation wavelength of 544 nm and an emission wavelength of 590 nm. To detect the binding specificity of PSMA-EMs-N and PSMA-EMs-L to PSMA protein, the samples were preincubated with 10 nM of free PSMA protein for 1 h at room temperature before adding to the wells.

PSMA expression in PC cell lines

C4-2B, LNCaP and PC3 cells were washed with PBS and detached using Versene (Life technologies, UK). Cells were centrifuged and washed using 1% BSA/PBS. Next, 1 x 10^6 cells were resuspended in 1 mL of 1% BSA/PBS and incubated with primary rabbit anti-PSMA antibody (1:1000; 12702S, Cell signalling) at room temperature for 3 h. Cells were washed three times with 1% BSA/PBS, and resuspended with anti-rabbit secondary antibody Alexa Fluor® 488 Conjugate (1:1000; 4412S, Cell Signalling) for 2 h in the dark at room temperature. Cells were washed again three times with 1% BSA/PBS and analysed using BD FACS Calibur™ (BD Biosciences). Ten thousand events were acquired in the gated cell population of interest. Cellular uptake was assessed by median fluorescence intensity (FL-1 detector was used for analysis). For western blot analysis, cells were lysed using RIPA buffer and 20 µg of protein was loaded to 10% SDS-PAGE gel. Western blot was performed as described previously, using primary antibody against PSMA (1:1000; 12702S, Cell signalling) and secondary HRP-conjugated anti-rabbit IgG (1:1000; 7074, Cell Signalling).

Uptake studies by flow cytometry

C4-2B, LNCaP and PC3 cells (6 x 10^4) were seeded in 24-well plates (Sarstedt) pre-coated with poly-D-lysine. After 72 h, cells were incubated in advanced RPMI 1640 medium supplemented with 5% serum, as recommended by the manufacturer, and 1 x 10^{10} particles/mL of DiI labelled EMs, PSMA-EMs-N and PSMA-EMs-L at 37 °C/5% CO_2. After 0.5, 1, 3 and 6 h, cells were washed with PBS, trypsinised, pelleted at 300 x g for 5 minutes, washed again, and resuspended in 0.2 mL of PBS. Dot plots and histograms were set using the BD FACS Calibur™ flow cytometer (Becton Dickinson) equipped with CellQuest Pro™ software (Becton Dickinson). Ten thousand events were acquired in the gated cell population of interest. Cellular uptake was assessed by DiI median fluorescence intensity (MFI). FL-2 detector was used for analysis.

Uptake studies by confocal laser scanning microscopy (CLSM)

C4-2B cells (3000 cells/well) were seeded overnight in complete media onto glass chamber slides (Fisher Scientific) pre-coated with poly-D-lysine. After 72 h, cells were incubated with Dil-labelled EMs, PSMA-EMs-N and PSMA-EMs-L at a concentration of 1 x 10^{10} particles/mL at 37 °C/5% CO_2. At different time points (1 and 3 h), cells were washed with PBS and fixed with 0.3 mL of 4% (v/v) paraformaldehyde in PBS (room temperature for 20 min in the dark). Cells were washed with PBS to remove fixative, then incubated with 0.3 mL of 1 µg/mL of Hoechst 33342 (ThermoFisher) for 10 min to allow nuclei visualisation. The coverslips were mounted on glass slides using ProLong™ Gold Antifade mounting media (Invitrogen Life Technologies). Confocal images were acquired with Leica SP5 microscope (Leica microsystems) using a 63x oil immersion objective and 405 nm and 543 nm laser detectors. Image analysis was performed using the Fiji ImageJ software.

Indocyanine green (ICG) labelling

Purified EMs were incubated overnight with 20 µg/mL of ICG at 37 °C and 100 rpm shaking [35]. The sample was purified from free ICG using a PD-10 column (GE Healthcare). Labelled EMs were concentrated using 10k MWCO Amicon Ultra-4 centrifugal units (Sigma Aldrich). The ICG labelled EMs were lysed using DMSO inside the well of 96-well plate and encapsulated ICG was quantified by absorbance measurement using FLUOstar® Omega plate reader (wavelength range from 400-1000nm). The quantity of ICG was calculated using a standard curve of free ICG in DMSO (concentration range 1- 7.5 µg/mL, R^2 = 0.9994). The number of particles and ICG amount (Figure S7) and fluorescence were comparable for all the samples injected *in vivo*.

In vivo **biodistribution experiments**

All animal experiments were performed in compliance with the U.K. Home Office (1989) Code of Practice for the housing and care of animals used in scientific procedures. NSG mice (7 – 10 weeks old) were caged in individually vented cages with free access to food and water. A temperature of 19-22 °C was maintained, with a relative humidity of 40 – 60% and a 12 h light/dark cycle. Three animals were used in each group (n=3). A week before the imaging studies all animals were put on a special Teklad Global 19% protein extruded rodent diet, 2919 (Envigo, UK). For the biodistribution studies, free ICG and ICG labelled EMs and PSMA-EMs-N (2 µg of ICG, ~ 4 x 10^{10} particles/animal in 200 µL) were injected intravenously via the tail vein of male NSG mice. 1, 2, 4 and 24 h post-injection, fluorescence in the whole body was measured by In-Vitro Xtreme II (Bruker, USA). At the end of the study, mice were sacrificed and ICG fluorescence was quantified in tissues including the heart, lungs, liver, spleen, kidneys, and reproductive system.

For tumour targeting studies, mice were anaesthetised with isoflurane and inoculated subcutaneously in the flank region with 5 x 10^6 (50 µL) C4-2B cells mixed with Corning® Matrigel® Matrix, high concentration (50 µL). Tumour volume was estimated by caliper measurement three to four times per week and calculated using the formula V = (W^2 × L)/2 where V is tumour volume, W is tumour width and L is tumour length. Biodistribution studies were performed when the tumour volume reached ~ 300 mm^3. Free ICG and ICG labelled EMs and PSMA-EMs-N (2 µg of ICG, ~ 4 x 10^{10} particles/animal in 200 µL) were injected via the tail vein, and fluorescence was visualised after 4 and 24 h using In-Vitro Xtreme II (Bruker, USA). The mice were sacrificed after 24 h to quantify the fluorescence intensity. Images were quantitatively analysed by drawing regions of interest (ROI) around the tumour region and tissues using Molecular Imaging software MI 7.5 (Bruker, USA).

Statistical analysis

The data were presented as mean ± SD (n represents the number of repeats). For *in vitro* studies, significant differences were examined using two-way ANOVA with Bonferroni post-hoc test. RT-PCR, binding studies and *in vivo* biodistribution data analysis was performed using student *t*-tests. Differences

between groups were considered to be significant at a p value of <0.05. Statistical analysis was performed with GraphPad Prism 7.0 (GraphPad Software, Inc., San Diego, CA).

3. Results

Expression of PSMA-targeting peptide on the surface of U937 cells

To generate anti-PSMA-peptide-expressing U937 cells (abbreviated as PSMA-U937 cells), two methods were used: namely, nucleofection and lentiviral transduction. U937 cells were first transfected using 4D Nucleofector™ electroporation device (Lonza Group, Switzerland), with a pDisplay™ plasmid cloned with WQPDTAHHWATL sequence. Proteins expressed from pDisplay™ are fused at the N-terminus to the murine Ig κ-chain leader sequence, which directs the protein to the secretory pathway, and at the C-terminus to the platelet derived growth factor receptor (PDGFR) transmembrane domain, which anchors the protein to the plasma membrane, displaying it on the extracellular side (**Figure S1.A**). 48 h post-nucleofection, Western blot was performed to detect the PSMA-binding peptide on U937 cells (**Figure S1.B**), using a monoclonal antibody against haemagglutinin A epitope tag (HA-Tag). A weak HA-Tag band was detected, indicating mixed populations of cells. To ensure the expression of the anti-PSMA peptide on all U937 cells, a PSMA-U937-N cell line was established by monoclonal selection in a medium containing geneticin antibiotic (500 μg/mL). Next, isolated colonies were expanded, and screened for the anti-PSMA peptide by Western blot, flow cytometry, and RT-qPCR. Cells isolated from colony 7 (C7) showed the highest level of PSMA-peptide, and therefore were used for PSMA-targeted EMs preparation (**Figure S1.C-E**).

PSMA-U937 cells were also engineered using lentiviral transduction. The whole PSMA-peptide display sequence was cloned into a transfer vector to ensure the gene expression on the cell surface. eGFP was used as a reporter gene to easily monitor successful transgene expression under the EF1A promoter (**Figure S2.A**). Transduced cells were outgrown in a selection medium containing puromycin antibiotic and imaged for eGFP positive cells. Our results showed that lentiviral transduction was successful, however, it was evident that the majority of the puromycin-resistant cells eGFP were negative. Therefore, eGFP positive cells were sorted using a cell sorter, then used for PSMA-targeted EMs preparation (**Figure S2.B**). As expected, the isolated eGFP-positive cells exhibited high expression levels of the PSMA-binding peptide compared to the unsorted cells, as confirmed by the Western blot (**Figure S2.C**).

Following the successful engineering of PSMA-U937 cell lines, the level of anti-PSMA-peptide expression was compared in nucleofected (PSMA-U937-N) and lentiviral transduced (PSMA-U937-L) cells (**Figure 1**). Both cell lines (PSMA-U937-L & PSMA-U937-N) showed higher protein levels of the anti-PSMA peptide, compared to the wild-type cells (U937-WT) (**Figure 1.A**). Surprisingly, despite the comparable anti-PSMA peptide expression in both engineered cell lines, the PSMA-U937-N cells

expressed almost two-fold higher levels of anti-PSMA-peptide mRNA to the PSMA-U937-L cells (**Figure 1.B**), which requires further investigation.

<div align="right">**Figure 1**</div>

Preparation and characterisation of PSMA-targeted EMs

Our EMs were engineered using serial extrusion cycles, as described previously [24]. Briefly, U937-WT cells were extruded to produce non-targeted EMs, while nucleofected and lentiviral transduced cells were used to prepare PSMA-targeted EMs: PSMA-EMs-N and PSMA-EMs-L, respectively. Following extrusion, EMs were purified from free proteins and debris using size exclusion chromatography (qEV, Izon Science), and characterised using DLS (size, polydispersity), laser Doppler electrophoresis (zeta potential) and NTA (size & particle concentration) (**Table 1**). As shown by DLS, all prepared EMs showed comparable average hydrodynamic diameter (170 – 180 nm), polydispersity index (< 0.2), and zeta potential (~ -18 mV), which indicated that the presence of anti-PSMA peptide on the cell surface did not affect the properties of the engineered EMs. To complement the DLS results, NTA measurements were also carried out. The NTA results confirmed the narrow and similar size distribution of all engineered EMs with a mean particle diameter ranging between 133 – 135 nm, and comparable particle concentrations (2.16 – 2.49 x 10^{10} particles/mL). As anticipated, the DLS measurement showed slightly bigger particle size than NTA, which was consistent with previously reported studies[36]. Finally, TEM microscopy revealed spherical structures of all three EMs (**Figure 2.A & Figure S3**).

<div align="right">**Table 1**</div>

Next, Western blotting was used to study the protein expression on the engineered EMs. Promisingly, all three EMs retained the membrane proteins (LFA-1) and exosome markers (Moesin, Tsg101 and CD63) from the U937 cells (**Figure 2.B**), as previously reported[24]. LFA-1 was not successfully detected by Western blot in U937 cells, probably due to insufficient protein amount in the cell lysate. On the other hand, EMs showed LFA-1 and a stronger and diffused CD63 signal, indicating the abundance of these membrane proteins in the engineered EMs. More importantly, HA-Tag was also detected in the EMs prepared from both PSMA-U937 cells, confirming the presence of the PSMA-targeting peptide **(Figure 2.C)**. It is worth mentioning that the step of extruding cells did not affect the expression of membrane proteins. However, the higher signals detected in the EMs samples versus whole cell lysate are attributed to the higher concentration of the membrane proteins in the EMs. The

majority of soluble proteins were removed from the EMs during the purification step, unlike the whole cell lysate sample.

To validate that the PSMA-targeting peptide was properly incorporated into the EMs membrane, assembled with a correct conformation, and still able to bind its PSMA receptor, the binding ability of the targeted EMs to the purified recombinant PSMA protein was analysed using binding assay. Our results showed that non-targeted and targeted EMs were labelled with fluorescent lipophilic dye DiI, and incubated with immobilised PSMA in the wells of 96-well plate for 2 h. Interestingly, both PSMA-EMs-N and PSMA-EMs-L prepared from PSMA-U937 cells successfully bound to the PSMA-coated wells compared to the non-targeted EMs **(Figure 2.D)**. Next, a competitive binding assay was carried out by pre-incubating the targeted EMs with different concentrations (5-20 nM) of the soluble PSMA protein for 1 h before binding to the immobilised PSMA in the plate. As shown in the **Figure 2.E**, a significant reduction in EMs binding (~40%) was observed following EMs incubation with 10 nM of the soluble PSMA protein, confirming the specificity of the peptide-protein interaction. Furthermore, it was evident that varying the concentrations of pre-incubated PSMA protein significantly influenced the degree of PSMA-EMs binding inhibition (**Figure S4**). Overall, the binding of both PSMA-EMs-N and PSMA-EMs-L showed comparable results, therefore both targeted EMs were studied *in vitro* to assess their cellular uptake in different PC cell lines.

Figure 2

PSMA-dependant uptake of targeted EMs *in vitro*

To assess the PSMA expression on the surface of different PC cell lines, PC3, LNCaP and C4-2B cells were incubated with an anti-PSMA primary antibody followed by a fluorescently labelled secondary antibody, and the cells were analysed using flow cytometry. **Figure 3.A** depicts the mean fluorescence intensity (MFI) ratio of antibody treated to untreated cells. As expected, the shift in fluorescence was observed only in PSMA positive LNCaP and C4-2B cells, where PC3 cell line did not show the presence of PSMA protein on the cellular surface. Western blot analysis also confirmed the absence of PSMA protein in PC3 cell line, compared to C4-2B and LNCaP cells (**Figure 3.B**).

Figure 3

Following assessing the PSMA levels in different PC cells, the cellular uptake of fluorescently DiI-labelled EMs, PSMA-EMs-N and PSMA-EMs-L (1 x 10^{10} particles/mL) in PC3, LNCaP and C4-2B cells was studied using flow cytometry (**Figure 3.C**). Both EMs and PSMA-EMs displayed a time-dependent level of internalisation in all PC cell lines, where higher uptake was observed at 3 and 6 h

post-incubation. No differences were observed in PC3 cells at all time points, due to the absence of PSMA expression. On the contrary, in PSMA positive LNCaP and C4-2B cells, both PSMA-EMs-N and PSMA-EMs-L showed significantly higher cellular uptake than EMs at 3 and 6 h post-incubation, confirming the PSMA-targeting. These results were observed in both serum-free (data not shown) and complete media (**Figure 3.C).** Confocal laser scanning microscopy (CLSM) was also performed to assess the EMs cellular uptake. C4-2B cells were incubated with DiI-labelled EMs, PSMA-EMs-N and PSMA-EMs-L at 37 °C for 1 and 3 h at a final concentration of 1 x 10^{10} particles/mL. Confocal images showed higher uptake of both PSMA-EMs, compared to non-targeted EMs, confirming the results obtained by flow cytometry (**Figure S5**). All in all, the flow cytometry data and CLSM results support our initial hypothesis that PSMA-targeting peptide could improve the intracellular uptake of EMs in PSMA positive PC cell lines. Despite our promising PSMA uptake results, further studies are required to evaluate membrane flipping phenomenon following the extrusion cycles and its effect on membrane proteins for cellular binding and trafficking purposes.

PSMA- targeted EMs bind to PSMA expressing tumours *in vivo*

Finally, EMs and PSMA-EMs-N were studied *in vivo* to evaluate their tumour targeting capabilities following systemic administration. PSMA-EMs-N were selected for our *in vivo* testing due to the higher safety of non-viral vectors in gene expression. For this purpose, free ICG and ICG-labelled EMs and PSMA-EMs-N were injected intravenously into non-tumour bearing NSG mice, and imaged at 1, 2, 4 and 24 h post-administration (**Figure 4.A**). Accumulation of free ICG was observed at early time points (1 – 4 h) in the liver region, while EMs and PSMA-EMs-N fluorescence signals were more dispersed with less liver uptake. Overall, EMs and PSMA-EMs-N had similar biodistribution profiles. Upon e*x-vivo* examination, liver and spleen were the main accumulation sites of free ICG, EMs and PSMA-EMs-N (**Figure 4.B**). The quantification of ICG in organs confirmed that the free ICG was eliminated through the liver in less than 24 h, compared to ICG loaded into EMs, which required more time to be eliminated from the body (**Figure 4.C**). The clear differences in the biodistribution of ICG-labelled EMs compared to free ICG, indicates relatively stable ICG loading into EMs ((**Figure S8**), however, labelling exosomes' membrane using chemical conjugation will be more favourable to perform quantitative pharmacokinetics to determine the *in vivo* behaviour of our PSMA-EMs [37].

We further examined if PSMA-EMs-N specifically bind to PSMA expressing tumours *in vivo*. ICG-labelled EMs and PSMA-EMs-N were injected via the tail vein into C4-2B NSG-xenograft-bearing mice, and the animals were imaged after 4 and 24 h post-injection. As shown in **Figure 4.D**, the fluorescence signals were detected mainly in the liver region at 4 h, while after 24 h most of the signals decreased due to ICG excretion and elimination. It is worth mentioning that C4-2B tumours were implanted on the flank of the mice, thus they were not visible in the abdominal view of the living mice.

Animals were sacrificed after 24 h and organs were excised and imaged. Promisingly, stronger signals from the PSMA-EMs-N were detected in the tumour xenograft compared to EMs signals (**Figure 4.E**). On the other hand, free ICG showed faster body clearance than ICG-labelled EMs, with no tumour targeting (**Figure 4.D**). Accelerated small molecule clearance and higher liver uptake of nanocarriers in tumour-bearing mice compared to healthy mice was reported previously [38, 39]. Quantification of the region of interest (ROI) showed similar degree of organ uptake, where low accumulation of EMs and PSMA-EMs-N was observed in heart and lungs, but increased signals in the liver, spleen, and kidneys. These findings indicate that EMs are also taken up by macrophages as demonstrated in the exosomes biodistribution studies [31, 41]. Most importantly, the accumulation at the tumour site of PSMA-EMs-N was significantly higher than animals injected with non-targeted EMs (**Figure 4.F**). Furthermore, similar tumour targeting findings were observed using Dil-labelled EMs (**Figure S9**). These data indicated that PSMA-targeted EMs may facilitate the delivery of therapeutics to PSMA expressing tumours *in vivo*.

Figure 4

4. Discussion

Prostate-specific membrane antigen (PSMA) has been a well-established target in PC for drug delivery and imaging. It is highly overexpressed in the advanced stages of PC, such as aggressive hormone-refractory PC [40]. Several clinical trials have exploited PSMA targeting to deliver small molecules and imaging agents to PC tissues in patients [13-16]. Amongst various PSMA targeting ligands (e.g. antibodies and aptamers), peptides have many advantages, such as their low molecular weight, high tissue permeability, great stability, and flexibility in conjugation [11]. It is known that PSMA enzymatic activity is elevated in PC, which accelerates the cancer progression [42], so ligands that block PSMA enzymatic activity could show high promises in managing PC [43]. Phage display technology has been used to screen and identify anti-PSMA peptides, such as KYLAYPDSVHIW and WQPDTAHHWATL, that could bind PSMA and inhibit its glutamate carboxypeptidase activity [12, 43]. Interestingly, in contrast to all other PSMA targeting ligands, cells could be easily engineered to stably express peptides on their surface, thus improving their targeting to PSMA-expressing PC [44]. In the present work, the WQPDTAHHWATL peptide, which specifically binds the catalytic site of PSMA and inhibits its enzymatic activity [12], was expressed on the surface of U937 cells to increase the selectivity of the engineered EMs to PSMA expressing cells. In the future, to improve PSMA-EMs binding further, we have identified new peptides GTIQPYPFSWGY (K_d=8.22 uM) and KYLAYPDSVHIW (K_d=14.36 uM) that have higher PSMA binding affinity than our expressed WQPDTAHHWATL peptide (K_d=23.57 uM) [11] which could expressed using our novel approach.

Exosomes are naturally secreted vesicles. They exhibit several advantages over synthetic nanocarriers, such as their intrinsic homing ability, high biocompatibility, minimal immunogenicity and low toxicity; however, their main obstacle for the clinical applications is their low yield after purification [45]. Jang et al. were the first to develop exosome mimetic nanovesicles by extruding cells suspension though filters, producing a 100-fold higher yield than conventionally purified exosomes, while maintaining exosome mimetics intrinsic targeting to tumours [24]. Similarly, Goh et al. showed that doxorubicin-loaded exosome mimetics preferentially target cancerous HeLa cells more than HEK293 cells, demonstrating their natural targeting ability to malignant cell lines [28]. The intrinsic targeting of both exosomes and exosome mimetics is a significant advantage compared to synthetic nanocarriers; however, to enhance their tissue specificity, active targeting could be implemented. The active targeting of exosomes has been reported using a wide range of targeting ligands. For instance, Ohno at al. genetically engineered GE11 peptide-expressing cells, producing GE11 peptide expressing exosomes that bind EGFR expressing breast cancer cells [46]. Tian et al. engineered iRGD peptide expressing cells, where iRGD-exosomes bound αv integrin receptors, and improved doxorubicin therapeutic efficacy *in vitro* an *in vivo* compared to non-targeted exosomes [47]. Besides, genetically-engineered cells that secret targeted exosomes, targeting peptides could be conjugated to the exosomes surface using bio-orthogonal chemistry. In support of this, c(RGDyK) peptide was chemically conjugated to the surface of curcumin-loaded exosomes to target the lesion regions of the ischemic brain *in vivo*, and suppress the inflammatory response [48]. Ye et al. described another exosomes functionalisation method based on the molecular recognition between exosomes phospholipids and ApoA-I mimetic peptides. The methotrexate (MTX)-loaded exosomes were conjugated with KLA-LDL peptide by simple coincubation which increased exosomes uptake in glioblastoma cells, and enhanced the therapeutic effect of MTX *in vivo* [49].

On the contrary to exosomes, active targeting of exosome mimetics has not been heavily explored. To date, one study has been published reporting the preparation of aptamer-grafted exosome mimetics by anchoring AS1411 aptamer conjugated to cholesterol-PEG into mouse dendritic cells membrane, where the stability of the anchored targeting ligand can be an issue [23]. In the current study, we have engineered, for the first time, anti-PSMA peptide-decorated exosome mimetics for advanced PC. Interestingly, our results showed the successful membrane expression of WQPDTAHHWATL peptide using viral and non-viral vectors (**Figure 1.A**). Although several studies report better gene expression using lentiviral particles, our nucleofection results demonstrated comparable expression of PSMA-peptide (**Figure 1.B**), which is advantageous, since nucleofection is simple, reproducible, and raises minimal safety concerns in patients [50]. Interestingly, our findings showed that our EMs preserved U937 membrane proteins and exosomal markers (**Figure 2.A**), as described by others [24]. Furthermore, the binding and the cellular uptake studies indicated the proper peptide orientation and accessibility to bind the PSMA receptors (**Figure 2.D, 2.E, Figure 3.B, and Figure S4**) [47], which

increased the specificity of our PSMA-EMs, compared to non-targeted EMs, to PSMA-expressing PC cells **(Figure 3.C)**. Nevertheless, additional studies are required to evaluate the exact orientation of membrane proteins and anti-PSMA peptide in PSMA-EMs. The mechanism and routes of exosomes uptake have been widely studied; thus, more research is required to understand what determines the specific mechanism of EMs uptake [51, 52]. More importantly, our PSMA-EMs showed superior tumour accumulation *in vivo* following intravenous administration (**Figure 4.E & 4.F**) without apparent toxicity. Additional studies are required to evaluate the EMs toxicity profile. All in all, our data suggest that PSMA-targeted EMs could enable scale-up production of targeted EMs for clinical applications. Furthermore, using our proposed approach, a wide range of targeting peptides can be expressed on the surface of different cells, producing a high yield of targeted EMs for a wide range of applications.

Conclusion

In this work, a PSMA-targeting peptide (WQPDTAHHWATL) was successfully engineered on the surface of exosome mimetics using the genetic engineering approach. Nucleofection and lentiviral transduction were used to express the PSMA-targeting peptide on the cellular surface of the parent U937 cells. The extrusion method generated the PSMA-EMs with incorporated targeting ligand, and their active targeting was confirmed *in vitro* and *in vivo*. Further *in vivo* studies should be carried out to assess the pharmacokinetics, safety, and therapeutic efficacy of our PSMA-EMs in advanced PC mouse models.

Acknowledgements

References

[1] M.S. Litwin, H.-J. Tan, The Diagnosis and Treatment of Prostate Cancer, JAMA, 317 (2017) 2532, https://doi.org/10.1001/jama.2017.7248

[2] G.L. Wright, C. Haley, L.M. Beckett, P.F. Schellhammer, Expression of prostate-specific membrane antigen in normal, benign, and malignant prostate tissues, Urologic Oncology: Seminars and Original Investigations, 1 (1995) 18-28, https://doi.org/10.1016/1078-1439(95)00002-Y

[3] M.I. Milowsky, D.M. Nanus, L. Kostakoglu, C.E. Sheehan, S. Vallabhajosula, S.J. Goldsmith, J.S. Ross, N.H. Bander, Vascular targeted therapy with anti-prostate-specific membrane antigen monoclonal antibody J591 in advanced solid tumors, Journal of Clinical Oncology, 25 (2007) 540-547, https://doi.org/10.1200/JCO.2006.07.8097

[4] M.J. Morris, N. Pandit-Taskar, C.R. Divgi, S. Bender, J.A. O'Donoghue, A. Nacca, P. Smith-Jones, L. Schwartz, S. Slovin, R. Finn, S. Larson, H.I. Scher, Phase I evaluation of J591 as a vascular targeting agent in progressive solid tumors, Clinical Cancer Research, 13 (2007) 2707-2713, https://doi.org/10.1158/1078-0432.CCR-06-2935

[5] A.E. Machulkin, D.A. Skvortsov, Y.A. Ivanenkov, A.P. Ber, V.M. Kavalchuk, V.A. Aladinskaya, A.A. Uspenskaya, R.R. Shafikov, E.A. Plotnikova, R.I. Yakubovskaya, E.A. Nimenko, N.U. Zyk, E.K. Beloglazkina, V.N. Zyk, V.E. Koteliansky, A.G. Majouga, Synthesis and biological evaluation of PSMA-targeting paclitaxel conjugates, Bioorg. Med. Chem. Lett., 29 (2019) 2229-2235, https://doi.org/10.1016/j.bmcl.2019.06.035

[6] S. Hema, S. Thambiraj, D.R. Shankaran, Nanoformulations for Targeted Drug Delivery to Prostate Cancer: An Overview, Journal of Nanoscience and Nanotechnology, 18 (2018) 5171-5191, https://doi.org/10.1166/jnn.2018.15420

[7] W. Xu, I.A. Siddiqui, M. Nihal, S. Pilla, K. Rosenthal, H. Mukhtar, S. Gong, Aptamer-conjugated and doxorubicin-loaded unimolecular micelles for targeted therapy of prostate cancer, Biomaterials, 34 (2013) 5244-5253, https://doi.org/10.1016/j.biomaterials.2013.03.006

[8] A. Mhaka, A.M. Gady, D.M. Rosen, K.M. Lo, S.D. Gillies, S.R. Denmeade, Use of methotrexate-based peptide substrates to characterize the substrate specificity of Prostate-Specific Membrane Antigen (PSMA), Cancer Biology and Therapy, 3 (2004) 551-558, https://doi.org/846 [pii]

[9] T.P. Thomas, A.K. Patri, A. Myc, M.T. Myaing, J.Y. Ye, T.B. Norris, J.R. Baker, In Vitro Targeting of Synthesized Antibody-Conjugated Dendrimer Nanoparticles, Biomacromolecules, 5 (2004) 2269-2274, https://doi.org/10.1021/bm049704h

[10] V.A. Fuchs, B.W.C. Tse, A.K. Pearce, M.-C. Yeh, N.L. Fletcher, S.S. Huang, W.D. Heston, A.K. Whittaker, P.J. Russell, K.J. Thurecht, Evaluation of Polymeric Nanomedicines Targeted to PSMA: Effect of Ligand on Targeting Efficiency, Biomacromolecules, 16 (2015) 3235-3247, https://doi.org/10.1021/acs.biomac.5b00913

[11] W. Jin, B. Qin, Z. Chen, H. Liu, A. Barve, K. Cheng, Discovery of PSMA-specific peptide ligands for targeted drug delivery, Int. J. Pharm., 513 (2016) 138-147, https://doi.org/10.1016/j.ijpharm.2016.08.048

[12] S. Aggarwal, P. Singh, O. Topaloglu, J.T. Isaacs, S.R. Denmeade, A Dimeric Peptide That Binds Selectively to Prostate-Specific Membrane Antigen and Inhibits its Enzymatic Activity, Cancer Research, 66 (2006) 9171-9177, https://doi.org/10.1158/0008-5472.CAN-06-1520

[13] M.S. Hofman, J. Violet, R.J. Hicks, J. Ferdinandus, S.P. Thang, T. Akhurst, A. Iravani, G. Kong, A. Ravi Kumar, D.G. Murphy, P. Eu, P. Jackson, M. Scalzo, S.G. Williams, S. Sandhu, [177Lu]-PSMA-617 radionuclide treatment in patients with metastatic castration-resistant prostate cancer (LuPSMA trial): a single-centre, single-arm, phase 2 study, The Lancet Oncology, 19 (2018) 825-833, https://doi.org/10.1016/S1470-2045(18)30198-0

[14] J.A. Barrett, R.E. Coleman, S.J. Goldsmith, S. Vallabhajosula, N.A. Petry, S. Cho, T. Armor, J.B. Stubbs, K.P. Maresca, M.G. Stabin, J.L. Joyal, W.C. Eckelman, J.W. Babich, First-in-man evaluation of 2 high-affinity PSMA-avid small molecules for imaging prostate cancer, Journal of Nuclear Medicine, 54 (2013) 380-387, https://doi.org/10.2967/jnumed.112.111203

[15] W.P. Fendler, S. Reinhardt, H. Ilhan, A. Delker, G. Böning, F.J. Gildehaus, C. Stief, P. Bartenstein, C. Gratzke, S. Lehner, A. Rominger, Preliminary experience with dosimetry, response and patient reported outcome after 177Lu-PSMA-617 therapy for metastatic castration-resistant prostate cancer, Oncotarget, 8 (2017) 3581-3590, https://doi.org/10.18632/oncotarget.12240

[16] J. Calais, J. Czernin, W.P. Fendler, D. Elashoff, N.G. Nickols, Randomized phase III trial of 68Ga-PSMA-11 PET/CT molecular imaging for prostate cancer salvage radiotherapy planning [PSMA-SRT], Journal of Clinical Oncology, 37 (2019) TPS136-TPS136, https://doi.org/10.1200/jco.2019.37.7_suppl.tps136

[17] S.M. Kim, H.S. Kim, Engineering of extracellular vesicles as drug delivery vehicles, Stem Cell Investigation, 4 (2017) 74, https://doi.org/10.21037/sci.2017.08.07

[18] P. Vader, X.O. Breakefield, M.J.A. Wood, Extracellular vesicles: Emerging targets for cancer therapy, Trends Mol. Med., 20 (2014) 385-393, https://doi.org/10.1016/j.molmed.2014.03.002

[19] Y. Toda, K. Takata, Y. Nakagawa, H. Kawakami, S. Fujioka, K. Kobayashi, Y. Hattori, Y. Kitamura, K. Akaji, E. Ashihara, Effective internalization of U251-MG-secreted exosomes into cancer cells and characterization of their lipid components, Biochem. Biophys. Res. Commun., 456 (2015) 768-773, https://doi.org/10.1016/j.bbrc.2014.12.015

[20] T.J. Smyth, J.S. Redzic, M.W. Graner, T.J. Anchordoquy, Examination of the specificity of tumor cell derived exosomes with tumor cells in vitro, Biochimica et Biophysica Acta (BBA) - Biomembranes, 1838 (2014) 2954-2965, https://doi.org/10.1016/j.bbamem.2014.07.026

[21] J.L. Hood, R.S. San, S.A. Wickline, Exosomes Released by Melanoma Cells Prepare Sentinel Lymph Nodes for Tumor Metastasis, Cancer Res., 71 (2011) 3792-3801, https://doi.org/10.1158/0008-5472.CAN-10-4455

[22] J.Z. Nordin, Y. Lee, P. Vader, I. Mäger, H.J. Johansson, W. Heusermann, O.P.B. Wiklander, M. Hällbrink, Y. Seow, J.J. Bultema, J. Gilthorpe, T. Davies, P.J. Fairchild, S. Gabrielsson, N.C. Meisner-Kober, J. Lehtiö, C.I.E. Smith, M.J.A. Wood, S.E.L. Andaloussi, Ultrafiltration with size-exclusion liquid chromatography for high yield isolation of extracellular vesicles preserving intact biophysical and functional properties, Nanomedicine: Nanotechnology, Biology and Medicine, 11 (2015) 879-883, https://doi.org/10.1016/j.nano.2015.01.003

[23] Y. Wan, L. Wang, C. Zhu, Q. Zheng, G. Wang, J. Tong, Y. Fang, Y. Xia, G. Cheng, X. He, S.-Y. Zheng, Aptamer-Conjugated Extracellular Nanovesicles for Targeted Drug Delivery, Cancer Res., 78 (2018) 798-808, https://doi.org/10.1158/0008-5472.CAN-17-2880

[24] S.C. Jang, O.Y. Kim, C.M. Yoon, D.-S. Choi, T.-Y. Roh, J. Park, J. Nilsson, J. Lötvall, Y.-K. Kim, Y.S. Gho, Bioinspired Exosome-Mimetic Nanovesicles for Targeted Delivery of Chemotherapeutics to Malignant Tumors, ACS Nano, 7 (2013) 7698-7710, https://doi.org/10.1021/nn402232g

[25] W. Jo, D. Jeong, J. Kim, S. Cho, S.C. Jang, C. Han, J.Y. Kang, Y.S. Gho, J. Park, Microfluidic fabrication of cell-derived nanovesicles as endogenous RNA carriers, Lab Chip, 14 (2014) 1261-1269, https://doi.org/10.1039/C3LC50993A

[26] Q. Zhao, B. Hai, X. Zhang, J. Xu, B. Koehler, F. Liu, Biomimetic nanovesicles made from iPS cell-derived mesenchymal stem cells for targeted therapy of triple-negative breast cancer, Nanomedicine: Nanotechnology, Biology and Medicine, 24 (2020) 102146, https://doi.org/10.1016/j.nano.2019.102146

[27] N.F. Ilahibaks, Z. Lei, E.A. Mol, A.K. Deshantri, L. Jiang, R.M. Schiffelers, P. Vader, J.P.G. Sluijter, Biofabrication of Cell-Derived Nanovesicles: A Potential Alternative to Extracellular Vesicles for Regenerative Medicine, Cells, 8 (2019) 1509, https://doi.org/10.3390/cells8121509

[28] W.J. Goh, C.K. Lee, S. Zou, E. Woon, B. Czarny, G. Pastorin, Doxorubicin-loaded cell-derived nanovesicles: an alternative targeted approach for anti-tumor therapy, Int. J. Nanomed., Volume 12 (2017) 2759-2767, https://doi.org/10.2147/IJN.S131786

[29] W. Jo, J. Kim, J. Yoon, D. Jeong, S. Cho, H. Jeong, Y.J. Yoon, S.C. Kim, Y.S. Gho, J. Park, Large-scale generation of cell-derived nanovesicles, Nanoscale, 6 (2014) 12056-12064, https://doi.org/10.1039/C4NR02391A

[30] K.-S. Park, K. Svennerholm, V.G. Shelke, E. Bandeira, C. Lässer, S.C. Jang, R. Chandode, I. Gribonika, J. Lötvall, Mesenchymal stromal cell-derived nanovesicles ameliorate bacterial outer membrane vesicle-induced sepsis via IL-10, Stem Cell Research & Therapy, 10 (2019) 231, https://doi.org/10.1186/s13287-019-1352-4

[31] W.J. Goh, S. Zou, W.Y. Ong, F. Torta, A.F. Alexandra, R.M. Schiffelers, G. Storm, J.-W. Wang, B. Czarny, G. Pastorin, Bioinspired Cell-Derived Nanovesicles versus Exosomes as Drug Delivery Systems: a Cost-Effective Alternative, Sci. Rep., 7 (2017) 14322, https://doi.org/10.1038/s41598-017-14725-x

[32] O.Y. Kim, S.J. Choi, S.C. Jang, K.S. Park, S.R. Kim, J.P. Choi, J.H. Lim, S.W. Lee, J. Park, D. Di Vizio, J. Lötvall, Y.K. Kim, Y.S. Gho, Bacterial protoplast-derived nanovesicles as vaccine delivery system against bacterial infection, Nano Lett., 15 (2015) 266-274, https://doi.org/10.1021/nl503508h

[33] T.R. Lunavat, S.C. Jang, L. Nilsson, H.T. Park, G. Repiska, C. Lässer, J.A. Nilsson, Y.S. Gho, J. Lötvall, RNAi delivery by exosome-mimetic nanovesicles – Implications for targeting c-Myc in cancer, Biomaterials, 102 (2016) 231-238, https://doi.org/10.1016/j.biomaterials.2016.06.024

[34] J.P.K. Armstrong, M.N. Holme, M.M. Stevens, Re-Engineering Extracellular Vesicles as Smart Nanoscale Therapeutics, ACS Nano, 11 (2017) 69-83, https://doi.org/10.1021/acsnano.6b07607

[35] F. Mao, Y. Wu, X. Tang, J. Kang, B. Zhang, Y. Yan, H. Qian, X. Zhang, W. Xu, Exosomes Derived from Human Umbilical Cord Mesenchymal Stem Cells Relieve Inflammatory Bowel Disease in Mice, BioMed Research International, 2017 (2017), https://doi.org/10.1155/2017/5356760

[36] V. Filipe, A. Hawe, W. Jiskoot, Critical evaluation of nanoparticle tracking analysis (NTA) by NanoSight for the measurement of nanoparticles and protein aggregates, Pharm. Res., 27 (2010) 796-810, https://doi.org/10.1007/s11095-010-0073-2

[37] L. Xu, F.N. Faruqu, R. Liam-or, O. Abu Abed, D. Li, K. Venner, R.J. Errington, H. Summers, J.T.-W. Wang, K.T. Al-Jamal, Design of experiment (DoE)-driven in vitro and in vivo uptake studies of exosomes for pancreatic cancer delivery enabled by copper-free click chemistry-based labelling, Journal of Extracellular Vesicles, 9 (2020) 1779458, https://doi.org/10.1080/20013078.2020.1779458

[38] M.P. Kai, H.E. Brighton, C.A. Fromen, T.W. Shen, J.C. Luft, Y.E. Luft, A.W. Keeler, G.R. Robbins, J.P.Y. Ting, W.C. Zamboni, J.E. Bear, J.M. Desimone, Tumor Presence Induces Global Immune Changes and Enhances Nanoparticle Clearance, ACS Nano, 10 (2016) 861-870, https://doi.org/10.1021/acsnano.5b05999

[39] G. Song, T.K. Tarrant, T.F. White, D.A. Barrow, C.M. Santos, R.G. Timoshchenko, S.K. Hanna, R.K. Ramanathan, C.R. Lee, V.L. Bae-Jump, P.A. Gehrig, W.C. Zamboni, Roles of chemokines CCL2 and CCL5 in the pharmacokinetics of PEGylated liposomal doxorubicin in vivo and in patients with recurrent epithelial ovarian cancer, 11 (2015) 1797-1807, https://doi.org/10.1016/j.nano.2015.05.007

[40] S.S. Chang, V.E. Reuter, W.D.W. Heston, P.B. Gaudin, Comparison of anti-prostate-specific membrane antigen antibodies and other immunomarkers in metastatic prostate carcinoma, Urology, 57 (2001) 1179-1183, https://doi.org/10.1016/S0090-4295(01)00983-9

[41] T. Imai, Y. Takahashi, M. Nishikawa, K. Kato, M. Morishita, T. Yamashita, A. Matsumoto, C. Charoenviriyakul, Y. Takakura, Macrophage-dependent clearance of systemically administered B16BL6-derived exosomes from the blood circulation in mice, Journal of Extracellular Vesicles, 4 (2015) 1-8, https://doi.org/10.3402/jev.v4.26238

[42] R.G. Lapidus, C.W. Tiffany, J.T. Isaacs, B.S. Slusher, Prostate-specific membrane antigen (PSMA) enzyme activity is elevated in prostate cancer cells, Prostate, 45 (2000) 350-354, https://doi.org/10.1002/1097-0045(20001201)45:4<350::AID-PROS10>3.0.CO;2-U

[43] J.P. Dassie, L.I. Hernandez, G.S. Thomas, M.E. Long, W.M. Rockey, C.A. Howell, Y. Chen, F.J. Hernandez, X.Y. Liu, M.E. Wilson, L.A. Allen, D.A. Vaena, D.K. Meyerholz, P.H. Giangrande, Targeted inhibition of prostate cancer metastases with an RNA aptamer to prostate-specific membrane antigen, Molecular Therapy, 22 (2014) 1910-1922, https://doi.org/10.1038/mt.2014.117

[44] P. Wu, T.A. Kudrolli, W.H. Chowdhury, M.M. Liu, R. Rodriguez, S.E. Lupold, Adenovirus targeting to prostate-specific membrane antigen through virus-displayed, semirandom peptide library screening, Cancer Res., 70 (2010) 9549-9553, https://doi.org/10.1158/0008-5472.CAN-10-1760

[45] X.C. Jiang, J.Q. Gao, Exosomes as novel bio-carriers for gene and drug delivery, Int. J. Pharm., 521 (2017) 167-175, https://doi.org/10.1016/j.ijpharm.2017.02.038

[46] S.-i. Ohno, M. Takanashi, K. Sudo, S. Ueda, A. Ishikawa, N. Matsuyama, K. Fujita, T. Mizutani, T. Ohgi, T. Ochiya, N. Gotoh, M. Kuroda, Systemically Injected Exosomes Targeted to EGFR Deliver Antitumor MicroRNA to Breast Cancer Cells, Molecular Therapy, 21 (2013) 185-191, https://doi.org/10.1038/mt.2012.180

[47] Y. Tian, S. Li, J. Song, T. Ji, M. Zhu, G.J. Anderson, J. Wei, G. Nie, A doxorubicin delivery platform using engineered natural membrane vesicle exosomes for targeted tumor therapy, Biomaterials, 35 (2014) 2383-2390, https://doi.org/10.1016/j.biomaterials.2013.11.083

[48] T. Tian, H.X. Zhang, C.P. He, S. Fan, Y.L. Zhu, C. Qi, N.P. Huang, Z.D. Xiao, Z.H. Lu, B.A. Tannous, J. Gao, Surface functionalized exosomes as targeted drug delivery vehicles for cerebral ischemia therapy, Biomaterials, 150 (2018) 137-149, https://doi.org/10.1016/j.biomaterials.2017.10.012

[49] Z. Ye, T. Zhang, W. He, H. Jin, C. Liu, Z. Yang, J. Ren, Methotrexate-Loaded Extracellular Vesicles Functionalized with Therapeutic and Targeted Peptides for the Treatment of Glioblastoma Multiforme, ACS Applied Materials and Interfaces, 10 (2018) 12341-12350, https://doi.org/10.1021/acsami.7b18135

[50] F. Cao, X. Xie, T. Gollan, L. Zhao, K. Narsinh, R.J. Lee, J.C. Wu, Comparison of gene-transfer efficiency in human embryonic stem cells, Molecular Imaging and Biology, 12 (2010) 15-24, https://doi.org/10.1007/s11307-009-0236-x

[51] A. Gonda, J. Kabagwira, G.N. Senthil, N.R. Wall, Internalization of exosomes through receptor-mediated endocytosis, Molecular Cancer Research, 17 (2019) 337-347, https://doi.org/10.1158/1541-7786.MCR-18-0891

[52] L.A. Mulcahy, R.C. Pink, D.R.F. Carter, Routes and mechanisms of extracellular vesicle uptake, Journal of Extracellular Vesicles, 3 (2014), https://doi.org/10.3402/jev.v3.24641
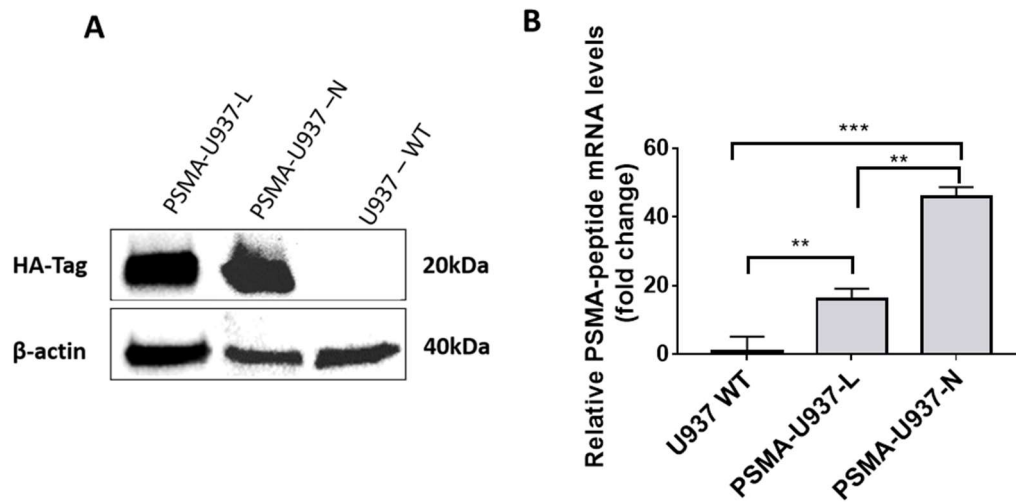
Figure 1. Engineering anti-PSMA-peptide-expressing U937 cells (PSMA-U937) using nucleofection and lentiviral transduction. (A) PSMA-U937 and U937-WT cells were lysed, and 20 µg of total protein was used for Western blotting. Anti-PSMA peptide expression was detected using anti-HA-Tag antibodies. **(B)** Anti-PSMA-peptide mRNA levels in PSMA-U937 cells were determined by RT-qPCR. mRNA levels were normalised by ACTB internal control and fold-change was calculated relative to U937-WT cells. Statistical significance was determined using multiple t-tests showing significant effects between U937-WT and PSMA-U937 cells (**, $p < 0.01$; ***, $p < 0.001$).
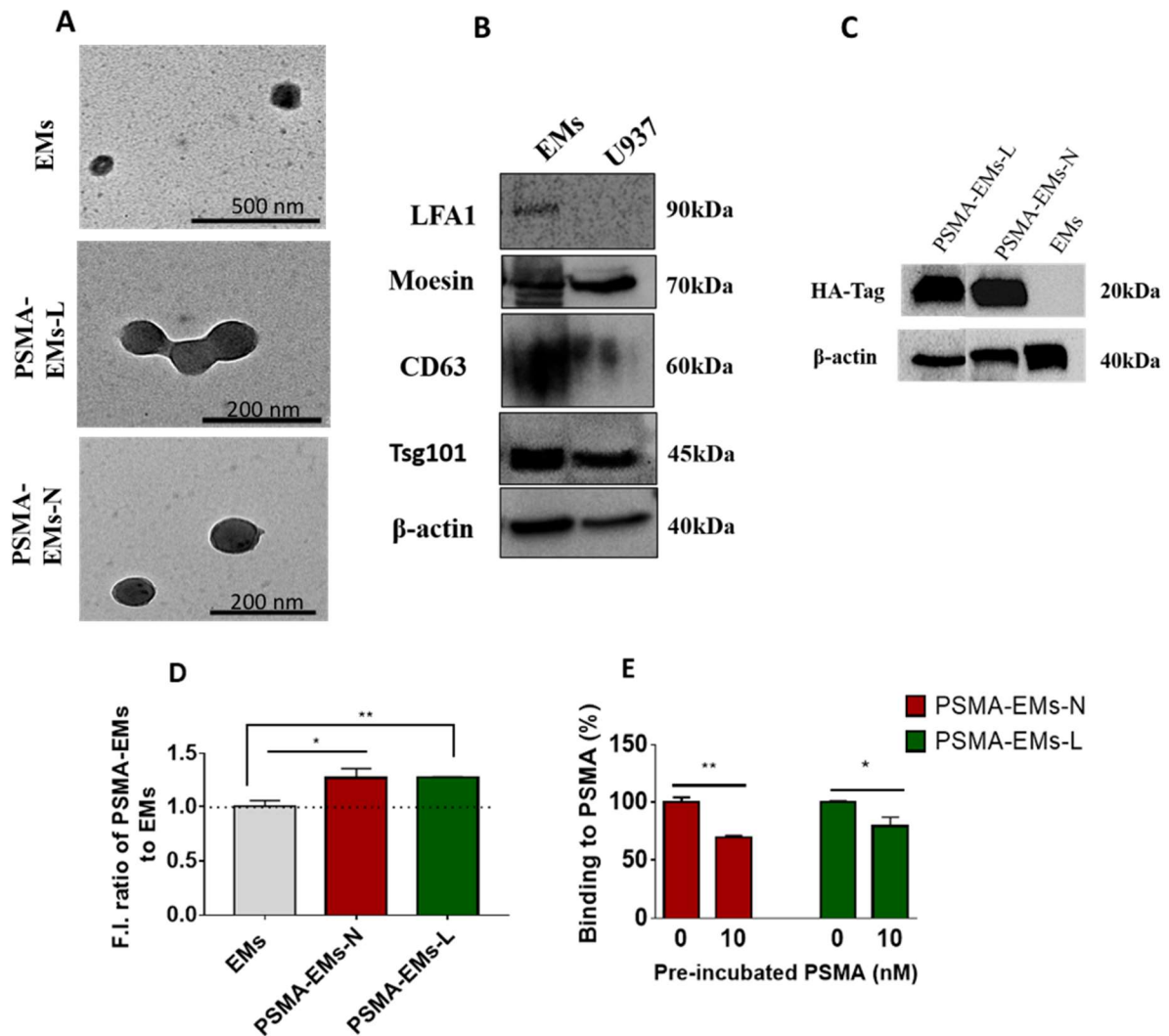
Figure 2. Morphological elucidation and protein characterisation of PSMA-targeted EMs. (**A**) TEM images of EMs, PSMA-EMs-L and PSMA-EMs-N extruded through 100 nm membrane using 5×10^6 cells/ mL and purified using a qEV column. Scale bar 500 nm & 200 nm (**B**) Western blot detection of exosomal markers (Moesin, Tsg101 and CD63) and a membrane protein (LFA1) on EMs and U937 cells. 20 µg of total protein was used for Western blotting. β-actin was used as a loading control. (**C**) Western blot detection of PSMA-targeting peptide (HA-Tag) on EMs prepared from PSMA-U937 cells. (**D**) Binding of DiI labelled EMs and PSMA-EMs at the concentration of 3.5×10^{10} particles/mL to immobilised PSMA protein was assessed by measuring the fluorescence intensity (F.I.) of the wells, followed by washing to remove unbound EMs. (**E**) Binding of PSMA-EMs was inhibited by the preincubation with 10 nM soluble PSMA for 1 h at room temperature. Each bar represents mean ± SD (n = 3). Statistical significance was determined using multiple t-tests showing significant effects between EMs and PSMA-EMs, or PSMA-EMs and pre-incubated samples with10 nM PSMA (*, $p < 0.05$; **, $p < 0.01$).
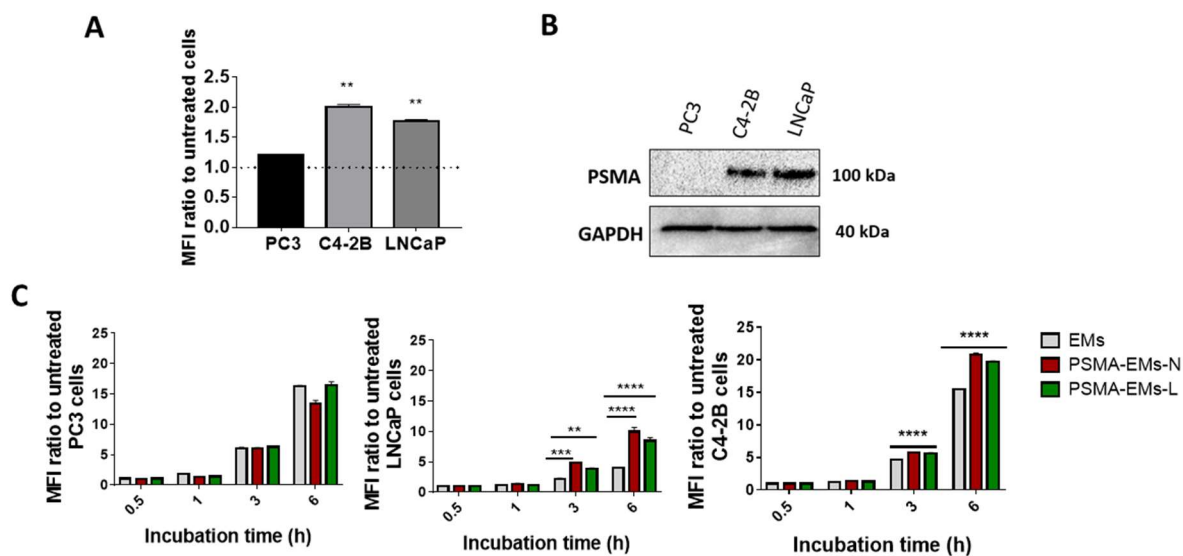
Figure 3. High cellular uptake of PSMA-EMs in PSMA-expressing cells. (A) PSMA expression in PC cell lines. Quantitative FACS analysis of PC3, C4-2B and LNCaP cells incubated with an anti-PSMA primary antibody and secondary anti-rabbit Alexa flour 488. The results are expressed as MFI ratio of the antibody treated to untreated cells. Each bar represents mean ± SD. **, $p < 0.01$ (ANOVA). **(B)** PSMA expression determined by Western blot. GAPDH was used as loading control. **(C)** Quantitative FACS analysis of PC3, C4-2B and LNCaP cells incubated with DiI-labelled targeted and non-targeted EMs at a particle concentration of 1×10^{10} particles/ mL for 0.5, 1, 3 and 6 h in complete media. Cells were incubated at 37 °C then trypsinised and washed for FACS analysis after each timepoint. The fluorescence of the lipophilic DiI dye was used as a measure of cellular uptake. Results are expressed as ratio of median fluorescence intensity (MFI) of treated cells to untreated cells ± SD (n = 3). Statistical significance was performed using one-way ANOVA showing significant effects between cells treated with EMs and cells treated with PSMA-EMs-N and PSMA-EMs-L (**, $p < 0.01$; ***, $p < 0.001$; ****, $p < 0.0001$).
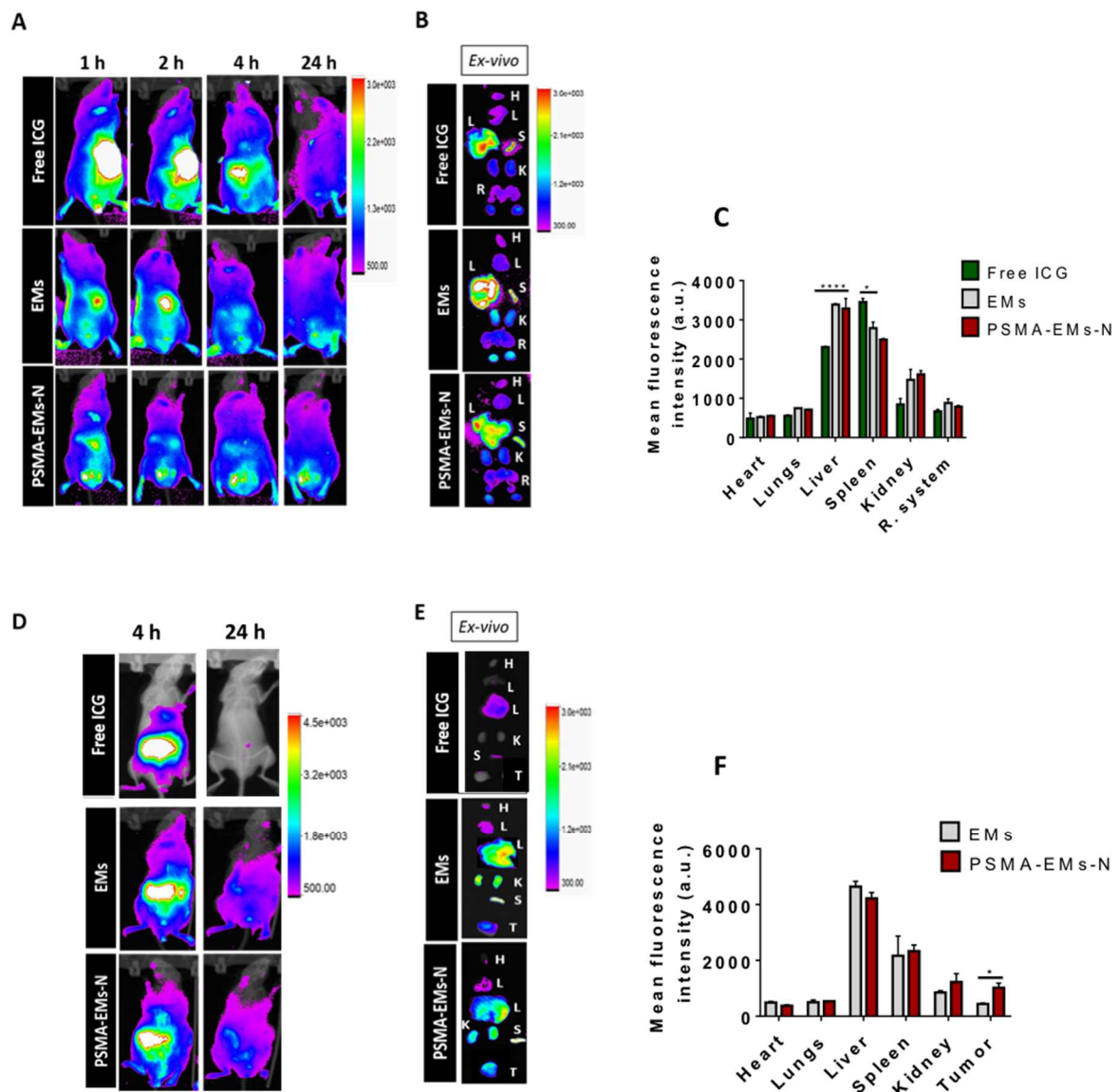
Figure 4. *In vivo* **biodistribution and higher tumour accumulation of PSMA-EMs-N in C4-2B tumour-bearing mice.**
(A) *In vivo* fluorescence imaging over 1, 2, 4 and 24 h post i.v. administration of free ICG, ICG labelled EMs and PSMA-ENs-N in non-tumour-bearing NSG mice. **(B)** *Ex vivo* image of the organs at 24 h post-administration. Heart (H), lungs (L), liver (L), kidneys (K), spleen (S), reproductive system (R). **(C)** Quantification of fluorescence intensity measured *ex vivo* in organs. Results are expressed as mean fluorescence intensity ± SD (n = 3). Statistical significance was measured using two-way ANOVA followed by Bonferroni's multiple comparisons test showing significant difference between free and encapsulated ICG (*, $p < 0.05$; ****, $p < 0.0001$). **(D)** *In vivo* fluorescence imaging (abdominal view) over 4 and 24 h post i.v. administration of free ICG or ICG labelled EMs in C4-2B tumour-bearing mice (tumours are not visible in the living mice since they were implanted on the back). **(E)** *Ex vivo* image of the organs and solid C4-2B tumours at 24 h following i.v. administration of ICG labelled EMs. Fluorescence signals demonstrating the biodistribution of injected EMs with greater uptake of targeted EMs at tumour site compared to non–targeted EMs. Heart (H), lungs (L), liver (L), kidneys (K), spleen (S), tumour (T). **(F)** Quantification of fluorescence intensity measured *ex vivo* in organs and solid tumours. Results are expressed as mean fluorescence intensity ± SD (n = 3). Statistical significance was measured using two-way ANOVA followed by Bonferroni's multiple comparisons test showing significant difference between EMs and PSMA-EMs accumulation in solid C4-2B tumour (*, $p < 0.05$).

Table 1. Physicochemical properties of PSMA-targeted EMs.

EMs Formulation	DLS & Laser Doppler electrophoresis			NTA	
	Z-ave ± SD (d. nm)	Pdl ± SD	ζ potential ± SD (mV)	Size ± SD (nm)	Concentration ± SD (particles/mL)
EMs	173.6 ± 4.843	0.184 ± 0.032	-18.3 ± 1.23	133.3 ± 2.055	$2.49 \times 10^{10} \pm 6.02 \times 10^{8}$
PSMA-EMs-N	172.6 ± 2.307	0.180 ± 0.035	-18.2 ± 2.47	135.6 ± 1.3	$2.26 \times 10^{10} \pm 5.67 \times 10^{8}$
PSMA-EMs-L	180 ± 6.037	0.092 ± 0.020	-19.5 ± 1.53	134.6 ± 2.4	$2.16 \times 10^{10} \pm 1.33 \times 10^{8}$